



HAL
open science

Plasma-sprayed coatings: Identification of plastic properties using macro-indentation and an inverse Levenberg–Marquardt method

Nora Kind, Bruno Berthel, Siegfried Fouvry, Cédric Poupon, Olivier Jaubert

► To cite this version:

Nora Kind, Bruno Berthel, Siegfried Fouvry, Cédric Poupon, Olivier Jaubert. Plasma-sprayed coatings: Identification of plastic properties using macro-indentation and an inverse Levenberg–Marquardt method. *Mechanics of Materials*, 2016, 98, pp.22-35. 10.1016/j.mechmat.2016.03.003 . hal-01523811

HAL Id: hal-01523811

<https://hal.science/hal-01523811>

Submitted on 17 May 2017

HAL is a multi-disciplinary open access archive for the deposit and dissemination of scientific research documents, whether they are published or not. The documents may come from teaching and research institutions in France or abroad, or from public or private research centers.

L'archive ouverte pluridisciplinaire **HAL**, est destinée au dépôt et à la diffusion de documents scientifiques de niveau recherche, publiés ou non, émanant des établissements d'enseignement et de recherche français ou étrangers, des laboratoires publics ou privés.

Plasma-sprayed coatings: Identification of Plastic properties using Macro-indentation and an inverse Levenberg-Marquardt method

N. Kind^{a,b}, B. Berthel^a, S. Fouvry^a, C. Poupon^b, O. Jaubert^b

^a : Laboratoire d Tribologie et Dynamique des Systèmes, UMR CNRS ECL ENISE ENSMSE 5513, Ecole Centrale de Lyon, 69134 Ecully cedex, France

^b : Airbus Operations S.A.S, 316 route de Bayonne, 31060 Toulouse, France

Plasma-sprayed coatings are widely used for thermal protection and wear stability of structural components. These coatings feature an anisotropic porous structure as a result of the thermal spraying process. Although current literature provides methods for the identification of elastic properties of these materials, to our knowledge little research is dedicated to describing their plastic behavior, especially when these coatings are subjected to macro-scale contacts encountered in industrial applications. In this work we present a novel inverse method for the identification of plastic properties of thick plasma-sprayed coatings by means of macro-indentation and finite element simulations coupled to a Levenberg-Marquardt optimization. This optimization aims to fit numerically generated residual indentation profiles to the experimentally obtained ones. For the description of the coatings' plastic behavior we made use of the Gurson-Tvergaard plasticity criterion coupled to a linear isotropic work hardening of the matrix. This criterion is appropriate for ductile porous solids as it takes into account the hydrostatic pressure, and it is readily implementable in commercial finite element software. The constitutive parameters to be identified include the yield strength σ_{y0} and the work hardening coefficient K of the solid matrix as well as two dimensionless fitting parameters q_1 and q_2 and the void fraction f . For the given plasma-sprayed coating we could show that the proposed method is capable of identifying these parameters after as little as three iterations where $\sigma_{y0} = 1624$ MPa, $K = 33340$ MPa, $q_1 = 3.29$, $q_2 = 4.60$ and $f = 4.2\%$.

Keywords: *macro-indentation, Gurson-Tvergaard plasticity, porous solids, Levenberg-Marquardt method, inverse identification, plasma-sprayed coatings*

Nomenclature

Symbol	Unit	Description
d	-	relative density
E_{IT}	Pa	Young's modulus as obtained by indentation
f	-	porosity volume fraction
g	-	search direction
K	Pa	work hardening coefficient
H_{IT}	Pa	Indentation hardness
q_1, q_2, q_3	-	Gurson-Tvergaard fitting parameters
n		strain hardening exponent
s		standard deviation
SNR		signal-to-noise ratio
$u_{x1}, u_{x2} \dots$	m	vertical displacement at coordinates $x_1, x_2 \dots$
α		step size
β	rad	angle of attack of indenter
ε_{ep}^p	-	equivalent plastic strain
λ	-	damping parameter
σ_m	Pa	hydrostatic pressure
σ_{yo}	Pa	yield strength in absence of voids
σ_{vm}	Pa	equivalent von Mises stress
ϕ	m	diameter
μ	-	friction coefficient

1. Introduction

Plasma-sprayed coatings are widely used for thermal protection and wear stability of components and their importance with respect to structural durability is significant. These coatings feature an anisotropic structure as a result of the thermal spraying process in which molten metal is projected onto a substrate at elevated speeds, leading to the formation of flatlike splats. Typically, these splats have diameters of 100-200 μm and exhibit thicknesses in the range of 2-10 μm [1]. The presence of lamellar microcracks and pores, often accompanied by the presence of oxides and other impurities, results in anisotropic porous microstructures with porosity volume fractions f amounting to 2-15% [4]. Whilst the influence of pores and microcracks on the coatings' elastic properties has been studied quite extensively, namely by Sevostianov et al. [1][2][3], to our knowledge few research activities aim to describe the plastic properties of these porous materials.

The purpose of this work is to propose a novel inverse method that identifies the plastic properties of plasma-sprayed coatings by means of macro-indentation and finite element simulations coupled to a Levenberg-Marquardt optimization.

Instrumented indentation techniques are commonly employed for the determination of hardness, elastic modulus, indentation toughness, tensile strength or fatigue and creep behavior [5]. The attractiveness of these techniques stems from the fact that material properties can be determined by simple analysis of the indentation load vs. displacement curve obtained in the course of indentation. Instrumented indentation can be performed at different length scales ranging from the nano to the macro scale. Whilst nanoindentation is commonly employed for the analysis of local phases or very thin films, macroindentation is useful for the study of a material's global behavior as the matter beneath the indenter can be assumed to be homogenous. In this study we consider highly anisotropic plasma-sprayed coatings. Macro-indentation seems to be the obvious choice for these materials if their plastic properties are to be described on a macroscopic scale.

The elastic-plastic properties of materials are commonly identified from the load displacement curve obtained in the course of indentation [12][13][14]. Although this common method is suitable for nano and microindentation, we propose an alternative method in this work. The inverse method

proposed in this study does not require knowledge of the entire loading history but it suffices to provide the geometry of the residual macro-indent. There are several advantages of this method compared to the traditional one:

- Knowledge of machine compliance is not necessary if the identification of plastic properties is based on the geometry of the residual indent only. This is in contrast to methods based on the load-displacement history since machine compliance strongly influences the precision of displacement measurements.
- Conventional methods based on the load-displacement history require knowledge of the real contact area between indenter and material which is mostly derived from the indentation depth according to the method developed by Oliver & Pharr [17][18]. The method proposed in this work avoids relating the penetration depth to projected contact area.
- The geometry of the residual indent provides information on the materials' hardening characteristics. This is exemplified by the formation of sink-in or pile-up regions around spherical indents in solids where the sink-in and pile-up phenomena are prevalent for materials exhibiting much strain hardening ($n > 0.2$ where n denotes the strain hardening exponent) and little strain hardening ($n < 0.2$), respectively [10][11]. Apart from the strain hardening characteristics, the formation of sink-in or pile-up is also influenced by contact friction and indentation depth [15].

In this paper the plastic properties of a Cobalt-based plasma-sprayed coating are determined using a novel inverse method that couples finite element simulations to experimental macro-indentations using a Levenberg-Marquardt algorithm. Section 2 of this article is meant to give an overview of the employed materials and experimental set-ups. We will see that the coating's plastic properties

can be described by the Gurson-Tvergaard plasticity criterion which is explained in section 3. The Levenberg-Marquardt method is described in section 4, followed by the presentation of the finite element model that is used to simulate the indentation process in section 5. The proposed method was validated by means of numerically generated solutions. This validation process is described in section 6 and it includes a sensitivity study of white noise, deviation on measurements and friction coefficient. Finally, the results are presented in section 7 of this paper.

2. Materials and experimental set-up

1.1 Coatings

The materials investigated in this study are Co-based coatings that are plasma-sprayed onto a 40CVD12 steel substrate. These coatings, depicted in Figure 1a, exhibit a thickness of approximately 140 μm . The heterogeneous coating is constituted of a solid phase (base alloy and oxides) and a porous phase (microcracks and large pores).

The porosity volume fraction of these coatings, hereafter denoted as f , can be estimated by image binarization of cross-sectional views obtained by optical imagery. Figure 1b depicts several binarized images of the same cross-section for different threshold values of contrast where the porous and solid phases are marked in white and black, respectively. One can see that the corresponding porosity volume fractions range between 1.3% and 9.2%. It is obvious that porosity volume fractions determined by this method are influenced to a significant extent by the choice of threshold value of contrast and they will differ to some extent between different cross-sectional views.

As will be shown in subsequent sections f has a significant influence on the plastic behavior of the coatings and it is of outmost importance to correctly determine this parameter. However, since f cannot be precisely determined using optical imagery, we have chosen this parameter to be one of the unknown variables to be identified using the proposed method.

As an initial guess for the Levenberg-Marquardt optimization we set $f_0=1.5\%$ considering that the seemingly porous spaces in between splats are mostly solid oxides and only the very dark cavities are actual porosities.

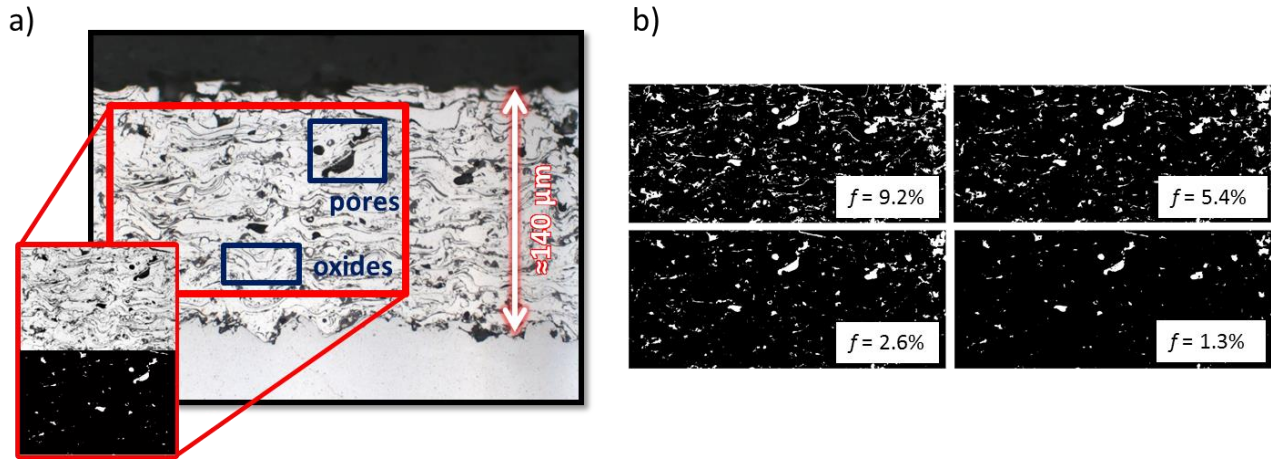


Figure 1 : (a) microstructure and (b) image binarization of optical images

1.2 Macro-indentation

In order to establish a macroscopic contact such as encountered in industrial applications we used a flat-ended conical indenter with a diameter of $\phi = 3.18\text{mm}$ made of 100C6 steel. The set-up used for macroindentation consists of a servo-hydraulic testing machine with a capacity of 100kN. The indentation loads for the flat-ended conical indenter ranges between 8-16kN. The servo-hydraulic testing machine and the close-up of the contact and indenter are depicted in figure 2.

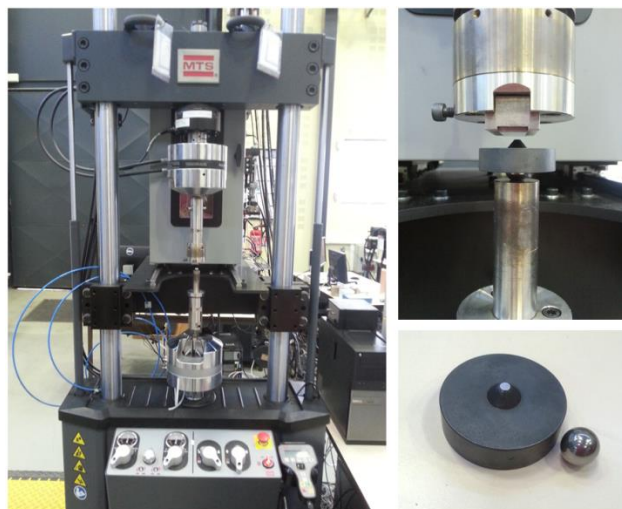


Figure 2 : experimental set-up for macro-indentation (left and right); indenter (bottom right)

The obtained indents are measured by profilometry making use of a Veeko non-contact profilometer at a magnification of 5 and a resolution of $1.97\mu\text{m}$. An example of the obtained 3D indentation profiles is depicted in figure 3a. Here, the indent was carried out at a load of 16000N. The Abaqus model associated with this problem is an axisymmetric model of the indenter-specimen-system which implies that the numerically computed indentation profiles are two-dimensional only. For the Levenberg-Marquardt algorithm to work, the 3D profiles obtained by profilometry need to be averaged around the indent's central axis in order to obtain a representative 2D profile. The averaged profile is depicted in figure 3b as a red line. The filtering of profilometric raw data as well as subsequent azimuthal averaging and smoothing strongly reduces the measurement noise.

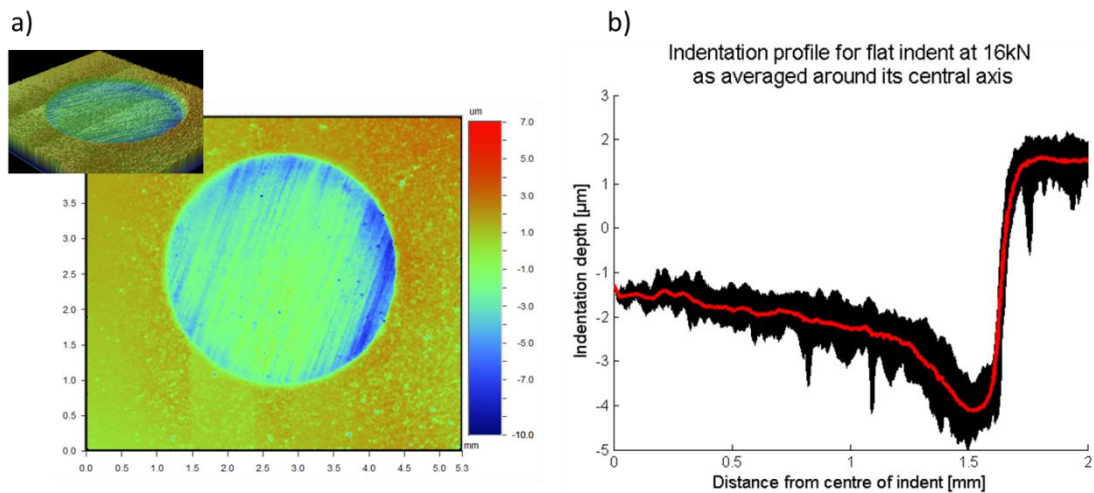


Figure 3 : a) 3D profilometry and b) azimuthal averaging of that profile around its central axis; red: average profile; black: sum of all profiles

Applying this procedure to all profilometric data of the indents, the indentation profiles depicted in figure 4 were obtained. The maximum indentation depth at the center of the indent amounts to approximately $3\mu\text{m}$ at a corresponding indentation load of 16kN. Furthermore it is important to note that only very little or almost no pile-up occurs at the edges of the indent which could be sign of significant strain hardening. We also observed relatively good repeatability of these tests; that is the deviation of indentation depth from an averaged depth over several tests amounts to a maximum of $0.06\mu\text{m}$. The effect of variation on measurements is discussed in section 6.3.

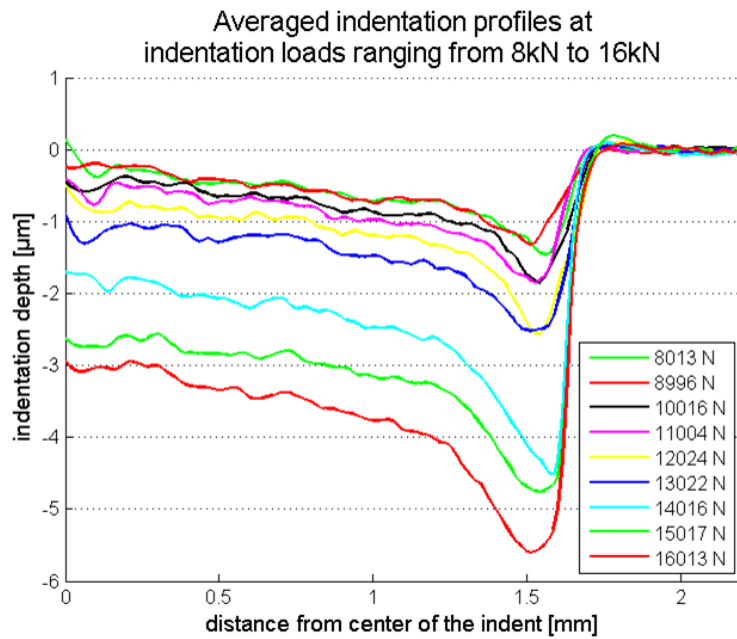


Figure 4 : indentation profiles after azimuthal averaging for flat indenter

1.3 Nano-indentation

It is possible to get a rough estimate of the solid phase's yield strength σ_{y0} and work hardening coefficient K using nano-indentation. The values of σ_{y0} and K obtained by means of nanoindentation serve as a reference to which the values obtained by the Levenberg-Marquardt method will be compared.

For nanoindentation we used a modified Berkovich and a cubecorner indenter exhibiting different representative strains within the material during loading. The representative strain ε during penetration is approximated as $\varepsilon = 0.2 \cdot \tan(\beta)$ where β is given by the angle of attack of the indenter [21]. For the modified Berkovich and cubecorner tips $\varepsilon_{Berkovich} = 6.8\%$ and $\varepsilon_{cubecorner} = 20.0\%$, respectively. The yield strength of solids can be approximated as $\sigma_y = H_{IT}/3.0$ where H_{IT} is the material hardness as determined by the method of Oliver and Pharr [17][18]. Making use of several indenters each exhibiting different representative strains, the materials' strain hardening behavior and yield strength at zero plastic strain can be reconstructed assuming a linear work hardening of the matrix. This method is illustrated in figure 5. More precisely, the parameters K and σ_{y0} are given by

$$K = \frac{\Delta y}{\Delta x} = \frac{\sigma_{cubecorner} - \sigma_{Berkovich}}{\varepsilon_{cubecorner} - \varepsilon_{Berkovich}} \quad (1)$$

$$\sigma_{y0} = \sigma_{Berkovich} - K\varepsilon_{Berkovich} = \sigma_{cubecorner} - K\varepsilon_{cubecorner} \quad (2)$$

In this study nanoindents were made at a maximum indentation load of 50mN and at a loading rate of 100mN/min for both the modified Berkovich and cubecorner indenter. A total of 30 indents were made for each indenter on both the cross-section of the coating and its top side. Table 1 gives an overview of the Young's modulus E_{IT} , hardness H_{IT} and yield strength σ_y obtained by means of nanoindentation as well as the standard deviation s of these parameters.

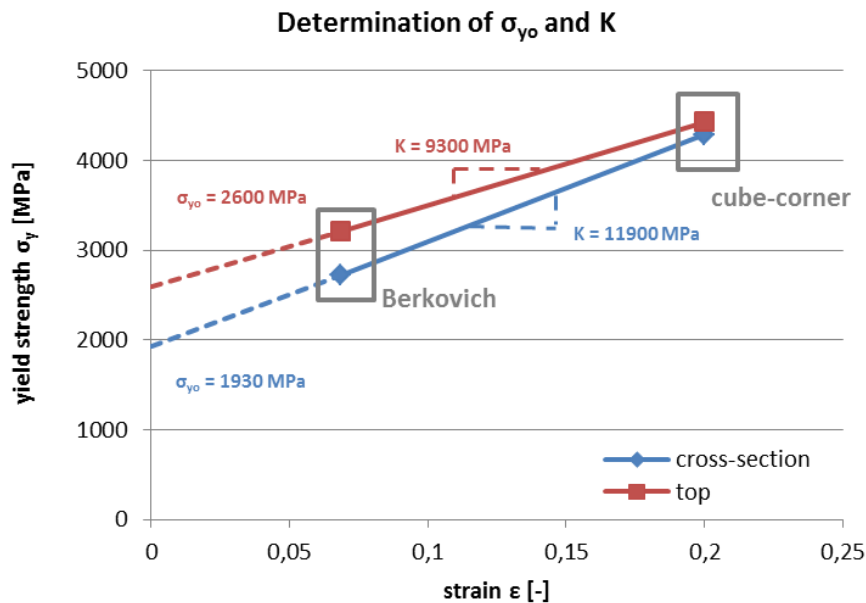


Figure 5: Determination of yield strength and work hardening coefficient

For the indents carried out on the cross-section and top side of the sample a work hardening coefficient K of approximately 11900MPa and 9300MPa was found, respectively. The yield strength σ_{y0} at 0.2% plastic strain can be obtained in a similar fashion assuming a linear work hardening. For the indents carried out on the cross-section and on the top side of the sample this parameter amounts to 2600MPa and 1930MPa, respectively. This influence of sample orientation on obtained yield strengths and work hardening coefficient illustrates well the materials'

heterogeneity. We will use $K_{top}=9300$ MPa and $\sigma_{y0,top}=1930$ MPa for comparison with results obtained by the Levenberg-Marquardt method.

Table 1 : Results nano-indentation ; s* = standard deviation

orientation	E [GPa] (s)*	H [MPa] (s)*	σ_y [MPa] (s)*
Top view			
Berkovich	127.5 (27)	9624 (2589)	3208.1 (863)
Cube-corner	147.9 (41)	13304 (2923)	4434.7 (975)
			$K_{top} = 9300$ MPa
			$\sigma_{y0,top} = 1930$ MPa
Cross-section			
Berkovich	124.2 (25)	8162 (1495)	2720.6 (498)
Cube-corner	172.1 (45)	14222 (3894)	4288.0 (1298)
			$K_{side} = 11900$ MPa
			$\sigma_{y0,side} = 2600$ MPa

3. Gurson-Tvergaard plasticity criterion

From the experimental indentation profiles in figure 4 it can be seen that indentation depths of up to $3\mu\text{m}$ can be obtained at the center of the indent. This deep indentation at the center can be explained by the closure of cracks and porosities under negative hydrostatic pressure. In order to sufficiently describe the plastic behavior of these coatings we therefore need a criterion that takes into account hydrostatic pressure. Furthermore, this criterion should be readily implementable in common finite element software. For these two reasons we have chosen the Gurson model as a first approach to this problem. In fact, this criterion, developed in 1977, is commonly used to describe the plastic behavior of porous ductile materials and therefore seems to be suitable.

In the Gurson model the matrix is taken as a continuum, obeying the von Mises yield criterion, where the effect of voids is averaged throughout the solid and where the porosity volume fraction f evolves with hydrostatic pressure. The yield function of the classical Gurson model is given as follows:

$$\Phi = \left(\frac{\sigma_{vm}}{\sigma_y}\right)^2 + 2f \cdot \cosh\left(-\frac{3}{2}\frac{\sigma_m}{\sigma_y}\right) - (1 + f^2) = 0 \quad (3)$$

Here, σ_{vm} is the equivalent von Mises stress, σ_y the uniaxial yield strength of the matrix in absence of voids, σ_m the hydrostatic pressure and f the porosity volume fraction of the solid. For a non-porous solid for which $f=0$, the Gurson criterion simply reduces to the von Mises yield criterion.

Tvergaard proposed a phenomenological extension of the original Gurson model in order to account for the interaction between voids and plastic work hardening by introduction of the non-dimensional fitting parameters q_1 , q_2 and q_3 . This model is known as the Gurson-Tvergaard model whose yield function is given by equation 4. The factors q_1 , q_2 are often assumed to take on values between $0 < q_1, q_2 < 1.5$ whilst q_3 is commonly approximated as $q_3 = q_1^2$. Although the Gurson-Tvergaard yield criterion was further extended by Needleman in order to account for void coalescence under tension, in this study we make use of the Gurson-Tvergaard model as the considered materials are deformed under compressive loads only.

$$\Phi = \left(\frac{\sigma_{vm}}{\sigma_y}\right)^2 + 2fq_1 \cosh\left(-\frac{3}{2}q_2 \frac{\sigma_m}{\sigma_y}\right) - (1 + q_3 f^2) = 0 \quad (4)$$

In the Gurson model and its extensions the solid matrix obeys the von Mises yield criterion. For this study we assumed the metallic matrix (without pores) to undergo linear work hardening where the work hardening exponent $n=1$. Although a power-law hardening ($n<1$) would be more appropriate to describe the matrix' yield behavior we used linear hardening as a first approach since it reduces the number of variables to be identified. Figure 6 depicts linear vs. power-law hardening. In fact, the elastic-plastic properties of plasma-sprayed coatings have previously been described by power-law relations [19][20].

$$\sigma_y = \sigma_{y0} + K \varepsilon_{eq}^{p^n} \quad (5)$$

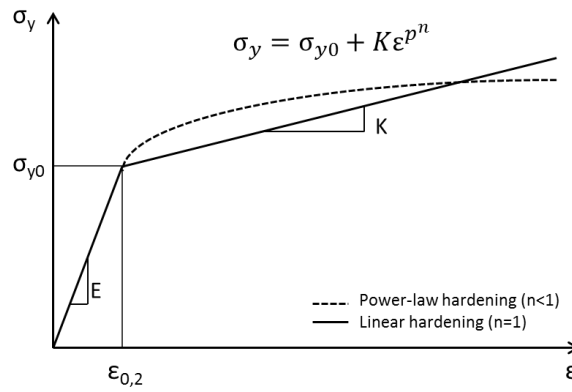


Figure 6: linear vs. power-law hardening

Here, σ_{y0} is the yield strength of the matrix in absence of voids, K the work hardening coefficient and ε_{eq}^p the equivalent plastic strain. From equations 4 and 5 one can see that the parameters to be identified are the non-dimensional fitting parameters q_1 and q_2 proper to the Gurson model as well as σ_{y0} and K of the solid matrix and the coatings' void fraction f . These parameters are all stored in the vector c .

$$c = (q_1, q_2, \sigma_{y0}, K, f)^T \quad (6)$$

Figure 7 illustrates well that using this criterion we can achieve non-zero indentation depths at the center for $f > 0.0\%$ whereas this is not possible for $f = 0.0\%$ (which reduces to the von Mises criterion) for an indentation load of $F = 15\text{kN}$, $\sigma_y = 1000\text{MPa}$, $K = 25000\text{MPa}$, $q_1 = 1.0$ and $q_2 = 1.5$.

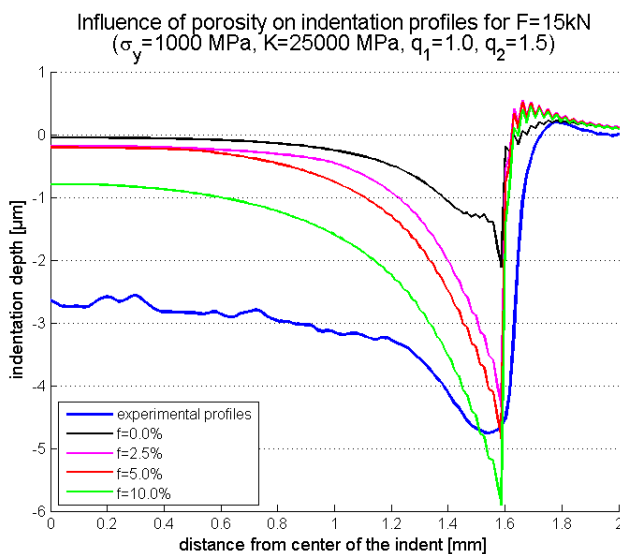


Figure 7 : indentation depths obtained by von Mises ($f=0.0\%$) vs. Gurson criterion ($f>0.0\%$)

4. Levenberg-Marquardt method

In order to solve for the vector $c = (q_1, q_2, \sigma_{y0}, K, f)^T$ of unknown material parameters we make use of the Levenberg-Marquardt method in combination with a parametric approximation to the problem. The Levenberg-Marquardt method is a standard technique for non-linear least-square problems combining features of the steepest descent method and the Gauss-method [6]: Whilst the algorithm behaves like a steepest descent method if the parameter guess is far from the solution (slow but guaranteed to converge), it behaves like a Gauss method if the parameter guess is close to it. The Levenberg-Marquardt algorithm aims to identify the vector c^* which minimizes the cost function $J(c)$ that can be expressed as the sum of squares of non-linear real-valued functions, representing the error between experimental and numerical results. In other words, c^* contains the parameter set for which the computed indent geometry comes closest to the experimental one; that is we would like to minimize the error between the vertical displacement obtained experimentally (U_n^{exp}) and numerically (U_n^{calc}). This error can be represented as either relative or absolute, depending on the problem at hand.

$$J(c) = \sum_{n=1}^N j_n^2(c) = \sum_{n=1}^N (U_n^{calc}(c) - U_n^{exp})^2 \quad (7)$$

$$J(c^*) = \min(J(c)) \quad (8)$$

Figure 8 illustrates the method of determining the cost function $J(c)$ by comparison of numerical and experimental indentation profiles.

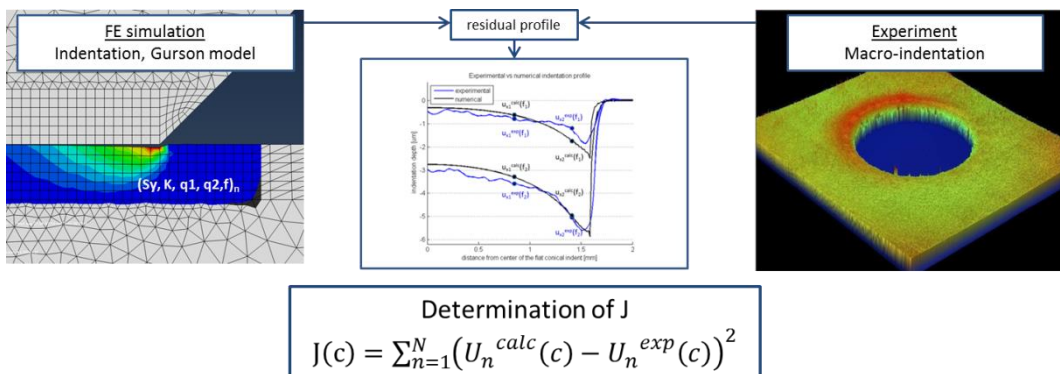


Figure 8 : Determination of cost function J by comparison of numerical and experimental indentation profiles

In order to guarantee convergence of the algorithm it is useful to have a rough idea of the solution space and to provide a meaningful initial parameter guess c^0 . We obtain the initial parameter guess $c^0 = (q_{1,0}, q_{2,0}, \sigma_{y0,0}, K_0, f_0)^T$ by means of a parametric approximation to the problem where we simulate the indentation problem by FEM for a certain number of parameter combinations. For this purpose we have considered the following ranges for the four parameters q_1 , q_2 , σ_{y0} and K (we set $f_0 = 1.5\%$ as discussed in section 2.1): $200\text{MPa} < \sigma_{y0} < 1500\text{MPa}$, $5000 < K < 30000\text{MPa}$, $0.5 < q_1 < 3.0$, $0.5 < q_2 < 3.0$. For these parameter ranges numerical indentation profiles can be generated and compared to those obtained experimentally. The parameter combination that leads to error minimization is used as an initial guess c^0 .

Subsequently the Levenberg-Marquardt algorithm is executed. In this optimization process the initial parameter guess c^0 is updated such that it minimizes the cost function $J(c)$ according to:

$$c^{k+1} = c^k + \alpha^k g^k \quad (9)$$

Here, α^k is the step size and g^k the search direction. The search direction g^k can be determined by knowledge of the first and second derivatives of the objective function using the following relations [8][9]:

$$g^k = -(A^T A + \lambda I)^{-1} \cdot A^T j \quad (10)$$

$$(\nabla_c J(c))_i = 2 \sum_{n=1}^N j_n(c) \frac{\partial j_n}{\partial c_i} = 2 A^T j \quad (11)$$

$$(H(c))_i = 2 \sum_{n=1}^N j_n(c) \frac{\partial j_n}{\partial c_i} \cdot \frac{\partial j_n}{\partial c_j} + j_n(c) \frac{\partial^2 j_n}{\partial c_i \partial c_j} \approx 2 \sum_{n=1}^N j_n(c) \frac{\partial j_n}{\partial c_i} = 2 A^T A \quad (12)$$

In the numerical implementation of the given problem the vector j is given as follows where u_{x1}^{calc} , u_{x2}^{calc} ... and u_{x1}^{exp} , u_{x2}^{exp} ... are the residual vertical displacements at different coordinates along the indentation profile x_1, x_2, \dots as determined from FEM simulation and from 3D profiling of the actual indent, respectively, for different indentation loads f_1, f_2 etc. The notation of the vertical displacements is illustrated by means of Figure 9.

$$j = \begin{pmatrix} \frac{u_{x1}^{exp}(f_1) - u_{x1}^{calc}(c^k, f_1)}{u_{x1}^{exp}(f_1)} \\ \dots \\ \dots \\ \frac{u_{x1}^{exp}(f_n) - u_{x1}^{calc}(c^k, f_n)}{u_{x1}^{exp}(f_n)} \\ \frac{u_{x2}^{exp}(f_1) - u_{x2}^{calc}(c^k, f_1)}{u_{x2}^{exp}(f_1)} \\ \dots \\ \dots \end{pmatrix} \quad (13)$$

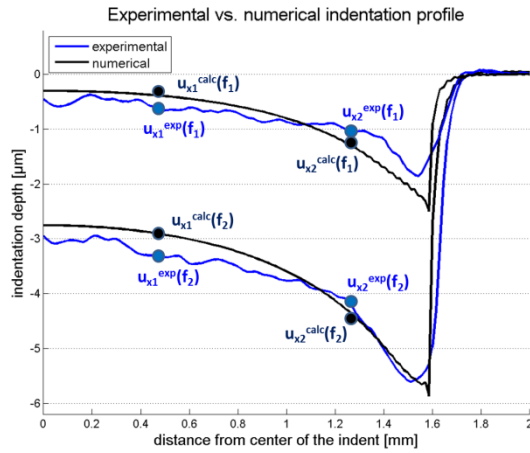


Figure 9 : definition of residual vertical displacements

Furthermore, the Jacobian A can be determined by finite differences of that vector, where c_i is represented by q_1, q_2, σ_{y0}, K or f :

$$\frac{\partial j_1^1}{\partial c_i}(c_1, \dots, c_i, \dots, c_n) \approx \frac{j_1^1(c_1, \dots, c_i + \alpha c_i, \dots, c_n) - j_1^1(c_1, \dots, c_n)}{\alpha c_i} \quad (14)$$

The damping parameter λ is adjusted in every iteration and initially set to a large value corresponding to a variable update according to the gradient descent method [7]. If the iteration results in a worse approximation to the solution, λ is increased and otherwise decreased, usually by the factors $\lambda_{up} = \lambda_{down} = 10$ [16]. As λ decreases, the Levenberg-Marquardt method approaches the Gauss-Newton method and typically converges rapidly towards a local minimum. The adjustment

of λ during iteration is controlled by the gain ratio R^k where λ is increased or decreased depending on the value of R^k [17], where $Q(c) = J(c^k) + (c - c^k)^T A^T j + \frac{1}{2} (c - c^k)^T (A^T A + \lambda I)(c - c^k)$.

$$R^k = \frac{J(c^k) - J(c^{k+1})}{Q(c^k) - Q(c^{k+1})} \quad (15)$$

The traditional scheme for updating λ is to multiply and divide its value by the same factor, say $\lambda_{up} = \lambda_{down} = 10$. In this study the less common updating scheme by *delayed gratification* was used which implies raising and lowering the value of λ by different amounts. We have found that $\lambda_{up} = 2$ and $\lambda_{down} = 10$ guarantees convergence. These findings are in agreement with the work of [16]. Figure 10 depicts the general flowchart of the optimization method that combines a parametric approximation with a Levenberg-Marquardt algorithm.

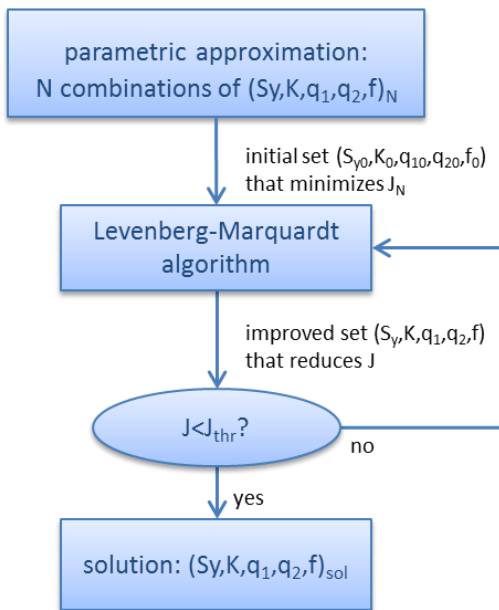


Figure 10: flowchart of optimization process

5. Finite element model

The finite element simulation of conical indentation was carried out using the commercial Abaqus 6.10 software. The components of the axisymmetric model are the indenter and the substrate-coating system. The flat-ended conical 100C6 steel indenter is modeled as a purely elastic solid

with an elastic modulus of $E=210$ GPa and a Poisson's ratio of $\nu=0.3$, having a diameter of $\phi=3.18$ mm as measured by profilometry. The substrate-coating system has been created by assigning the corresponding material properties to different sections of the same part where the substrate is an elastic-plastic material with $E=210$ GPa. For the contact between indenter and coating a friction coefficient of $\mu=0.5$ was measured.

The finite element model used to identify the coating's plastic properties is depicted in figure 11. The minimum element size in the vicinity of the contact amounts to approximately $15\mu\text{m}$. Elements further away from the contact were increased in size in order to reduce computation time. The indenter and substrate-coating system were meshed using four-node axisymmetric CAX4R and threenode axisymmetric CAX3 elements. For the Levenberg-Marquardt optimization we retrieve the vertical displacements u_{x1} , u_{x2} etc. of the surface nodes in the vicinity of the contact. The number of surface nodes amounts to 168.

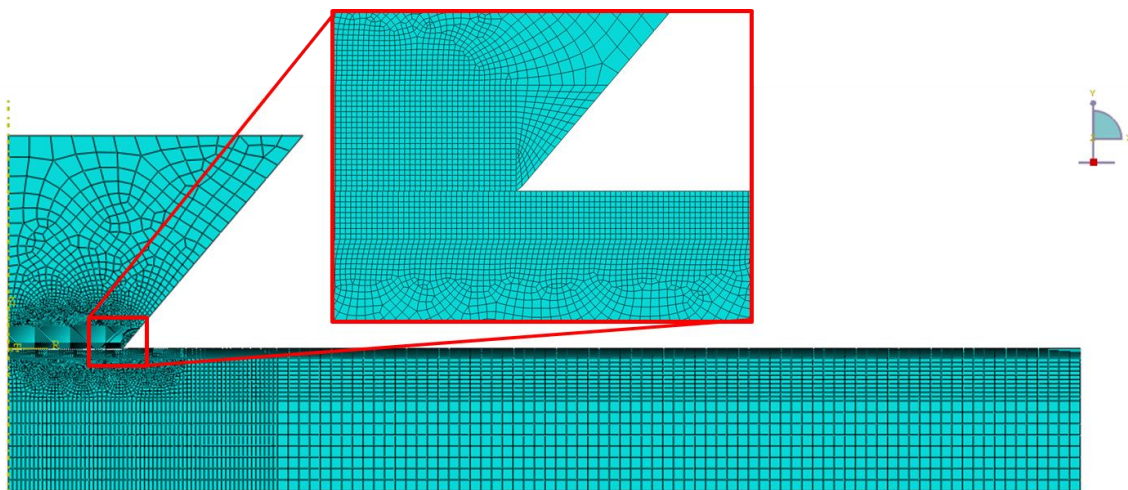


Figure 11 : finite element model for the conical indenter

Hereafter it will be shown in how far the minimum element size influences the shape of the obtained residual indentation profiles. Profiles were computed for an element size in vicinity of the contact of $10\mu\text{m}$, $15\mu\text{m}$, $20\mu\text{m}$, $30\mu\text{m}$, $40\mu\text{m}$ and $80\mu\text{m}$ for indentation loads in the range of 10kN to 16kN. Figures 12 and 13 depict the corresponding profiles for an indentation load of 16kN as well as the maximum indentation depth and indentation depth at the center of the indent. Whilst indentation profiles for mesh sizes above $20\mu\text{m}$ are discontinuous this is no longer the case for profiles created with mesh sizes below and including $20\mu\text{m}$. For this study we chose a mesh with a

minimum element size of 15 μm since it yields a smooth indentation profile and does not consume too much computational time. All calculations were made by use of a personal computer (dual core Intel® Core™ i5-3210M CPU at 2.5GHz, 8GB RAM, 64 bits Windows 7 Entreprise operating system). Typical processing times required to compute the indentation process for several loads are given in table 2. Processing times increase steadily for a refined mesh.

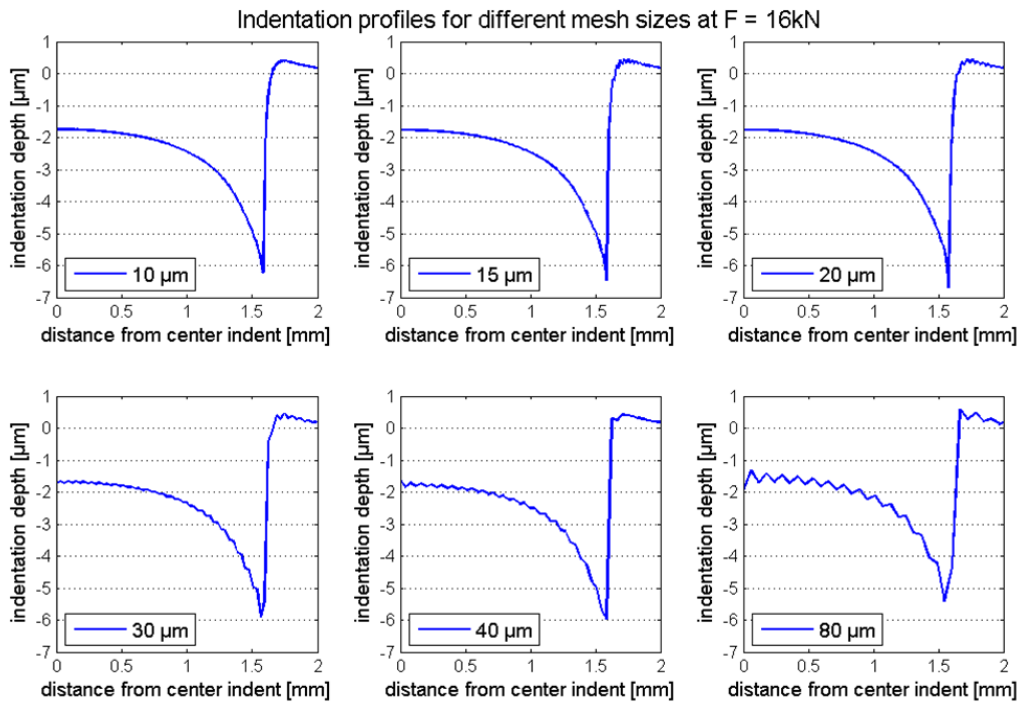


Figure 12: influence of mesh size on profiles

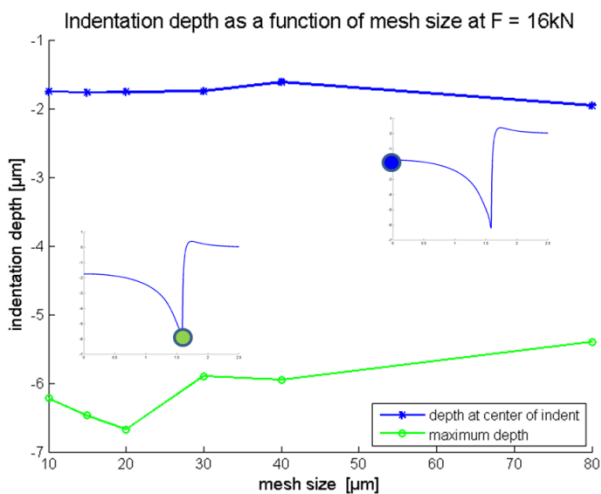


Figure 13 : Influence of mesh size on indentation depth

Table 2: Influence of mesh size on processing time

Mesh size [μm]	Processing time [s]
10	240
15	212
20	190
30	160
40	150
80	135

6. Numerical validation of the method

The Levenberg-Marquardt algorithm is validated by means of numerically generated reference profiles for a known set of parameters (σ_{y0} , K , q_1 , q_2 , d) where $\sigma_{y0} = 1000\text{MPa}$, $K = 20000\text{MPa}$, $q_1 = 3.0$, $q_2 = 3.0$ and $d = 0.985$ ($f = 1-d = 1.5\%$). This algorithm was validated for a large range of values for the porosity volume fraction but here we only show the results for a realistic porosity volume fraction that is close to 1.5%. The Abaqus model used for validation purposes is the one depicted in figure 11. The reference profiles were created for a set of five indentation loads: 10kN, 12kN, 14kN, 15kN and 16kN. These loads were chosen in accordance with our experimental data; that is the experimental profiles that are used for the identification of material parameters were obtained at those loads.

Table 3: Material parameters used for the generation of reference profiles

Generation of reference profiles		
Coating's plastic properties	σ_{y0}	1000MPa
	K	20000MPa
	q_1	3.0
	q_2	3.0
	d	0.985
Indentation load	10kN, 12kN,14kN,15kN,16kN	

In order to verify sufficient convergence of the Levenberg-Marquardt method, the initial parameter sets were chosen to be more or less far from the solution; that is by a maximum of 15%. The choice of a maximum divergence from the target value of 15% was made because we have a rough idea of the range for all parameters after the parametric approximation. Table 4 gives the numerical test conditions in terms of percentage divergence of initial parameters from the solution as well as the relative errors after a number of iterations. The results of a selection of convergence tests are depicted in more detail in figure 14. From these figures one can see that convergence of most parameters can be achieved within a maximum number of iterations of less than 15. More specifically it can be seen from figure 14 that all material parameters (except for q_1) approach the solution to a sufficient extent after the 5th iteration already. However, whilst the relative errors of

identified parameters are very low for σ_{y0} , K , q_2 and d with a maximum value of 3.44% for q_2 (test 4), the relative error for q_1 is relatively large with a maximum value as high as 16.94% (test 4). As a result, the value of q_1 as identified by the proposed method is not very reliable. The number of indentation profiles for which the material parameters are to be identified should be increased in order to improve convergence of this parameter.

Table 4: Convergence test results

Test	deviation of initial parameters					Relative error of identified parameters [%]				
	σ_{y0}	K	q_1	q_2	d	σ_{y0}	K	q_1	q_2	d
1	-10%	-10%	-10%	-10%	-10%	0.00	0.00	0.01	0.00	0.00
2	+10%	+10%	+10%	+10%	-10%	0.39	0.35	3.14	0.69	0.00
3	-15%	-15%	-15%	-15%	-15%	0.00	0.00	0.01	0.00	0.00
4	-10%	-10%	+10%	+10%	-10%	1.95	1.69	16.94	3.44	0.01
5	+10%	+10%	-10%	-10%	-10%	0.00	0.01	0.00	0.00	0.00
6	+15%	+15%	-15%	-15%	-15%	1.12	1.01	9.46	1.96	0.00
7	-5%	-5%	-5%	-5%	-5%	0.09	0.09	0.60	0.11	0.00
8	+5%	+5%	+5%	+5%	-5%	0.00	0.01	0.02	0.00	0.00

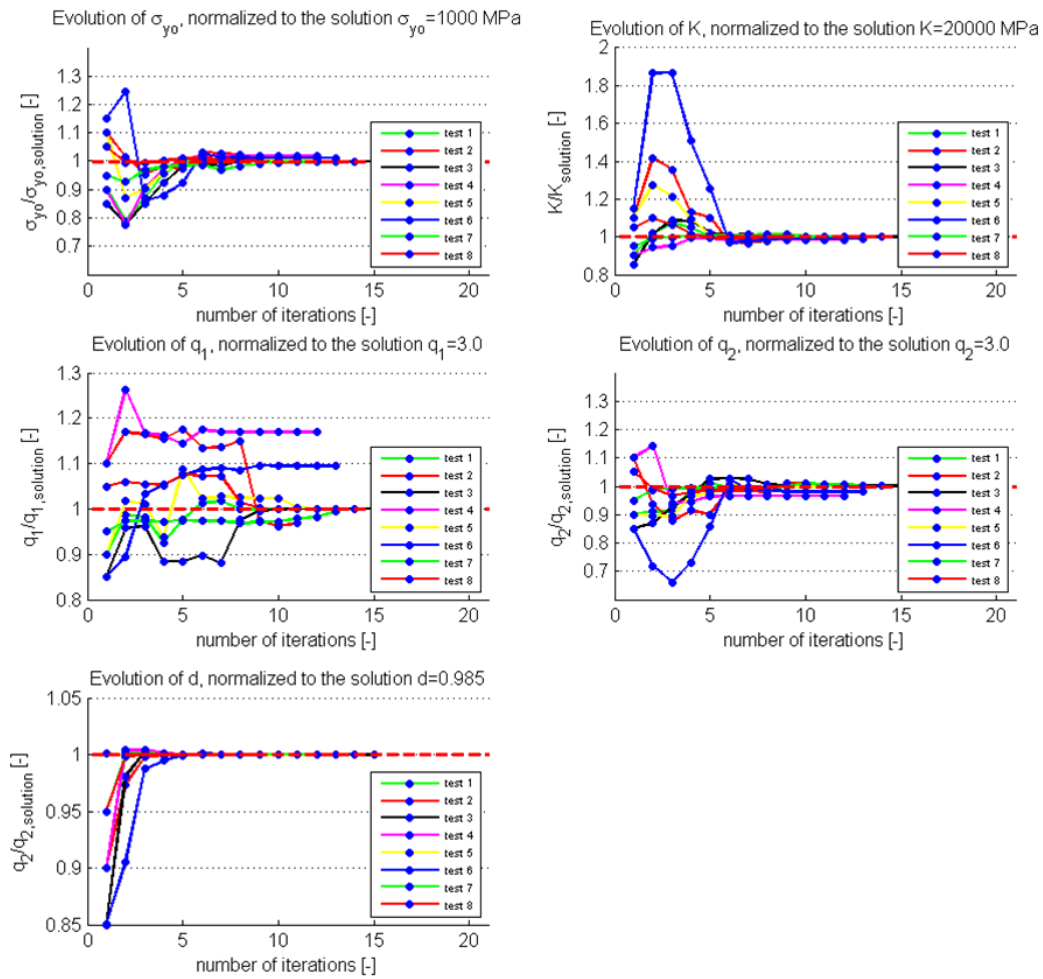


Figure 14: convergence performance of algorithm for all parameters

Figure 15 illustrates the convergence of the algorithm in terms of the indentation profile. The depicted profile corresponds to convergence test #6 at an indentation load of 16000N. It is obvious that as quickly as after 2 iterations the generated profile is very close to the reference profile. It should also be noted that the algorithm converges although there is an absolute difference between the initial profile and the solution of as much as 10 μ m.

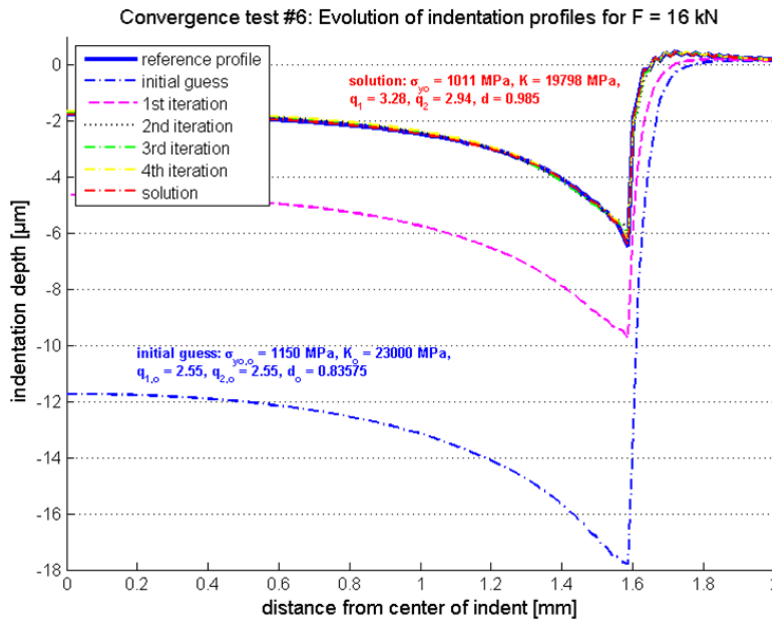


Figure 15: convergence of indentation profile towards solution

6.1 Influence of friction coefficient

The proposed method assumes knowledge of the coating's friction coefficient which, in this study, was measured as $\mu = 0.5$. We have determined the influence of a wrong estimation of the friction coefficient on the inverse parameter identification. For this purpose we have taken the initial parameter set corresponding to test#1 where $\sigma_{y0} = 900$ MPa, $K_o = 18000$ MPa, $q_{1,0} = q_{2,0} = 2.7$ and $d_o = 0.9865$. The reference profiles have been generated for a friction coefficient of $\mu = 0.5$. The following table shows in how far a deviation of this target value influences the parameter identification. From table 5 it becomes apparent the relative errors of identified parameters are relatively low with values ranging between 0.0% and 6.9%. Furthermore it is striking that the

highest errors, though acceptably low, occur for the parameter q_1 . This result again is in line with the convergence tests which have shown that the identification of q_1 is not very reliable.

Table 5 : influence of deviation of friction coefficient on identified parameters

Test	μ	Relative error of identified parameters [%]				
		σ_{y0}	K	q_1	q_2	d
1.1	0.3	3.90	3.08	6.59	1.94	0.03
1.2	0.4	0.34	0.50	4.69	1.31	0.00
1.3	0.6	3.99	2.71	6.90	1.88	0.02
1.4	0.7	0.82	1.05	6.27	1.31	0.00

6.2 Influence of scatter

Since the experimentally obtained indentation profiles are not very smooth but on the contrary are subject to irregularities we have studied the influence of adding white noise to the reference profiles. Figure 16 depicts noisy profiles that were generated for signal-to-noise ratios of 0.90, 0.85, 0.80, 0.75 and 0.70. In table 6 the associated results are given.

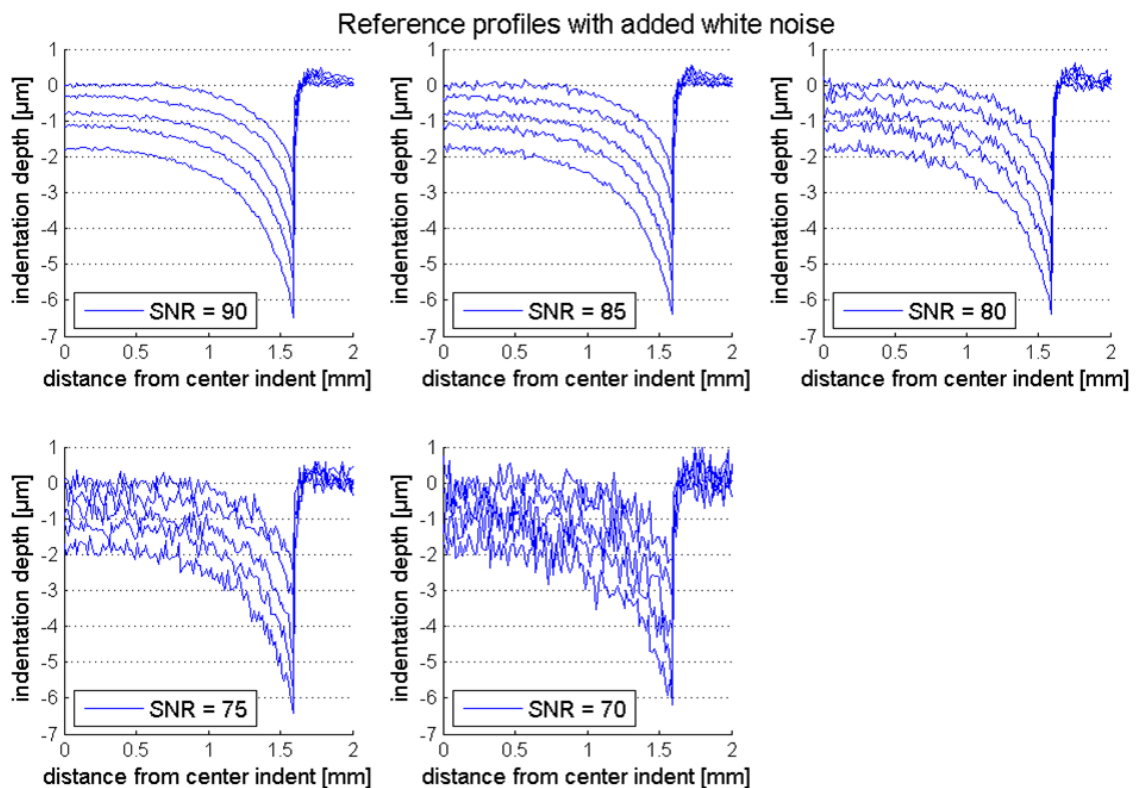


Figure 16: reference profiles with added white noise of SNR=90,85,80,75,70

Table 6 : Influence of white noise on parameter identification

Test	SNR	Relative error of identified parameters [%]				
		σ_{y0}	K	q_1	q_2	d
1.5	90	0.33	0.28	7.35	2.46	0.01
1.6	85	2.49	2.69	6.52	0.28	0.03
1.7	80	1.85	3.67	23.37	6.29	0.01
1.8	75	4.21	6.94	0.72	5.23	0.02
1.9	70	13.48	15.81	79.69	28.79	0.01

From the results presented in table 6 the following can be concluded: First of all the porosity volume fraction d is identified with high precision even for large signal-to-noise ratios. This observation again undermines the fact that porosity is the factor that mostly influences the shape of the residual profile. It also seems that all parameters except for q_1 can be determined sufficiently well up to a signal-to-noise ratio of $SNR = 75$. Below that value, that is for $SNR=70$, the noisy profiles are insufficient for inverse identification of parameters. The profiles corresponding to this very low value of $SNR=70$ are much more perturbed than the experimental profiles (figure 4). In other words, the experimental profiles' irregularity would rather correspond to a noisy profile of $SNR=85$ or $SNR=80$ for which the material parameters are identified sufficiently well. For this reason we can conclude the irregular shape of the experimental profiles to have a limited influence on the obtained results.

6.3 Influence of variation in measurements

When experimentally repeating an indentation experiment for the same conditions (temperature, load, indenter) we observed relatively good repeatability of these tests; that is the deviation of indentation depth from an averaged indentation depth over several tests amounts to a maximum of $0.06\mu\text{m}$. We have reproduced the effect of variation in measurements by shifting the indentation curves up or down by a random value within the limits of $0.06\mu\text{m}$. An example of such a randomly generated set of indentation profiles is depicted in figure 17 (corresponding to set 3 of table 7).

We generated 5 random sets of shifted profiles for which the results are given in table 8. Here again we can see that the porosity volume fraction d is very well identified. Also the parameters σ_{y0} and q_2 are sufficiently well identified. The largest errors occur again for the parameter q_1 .

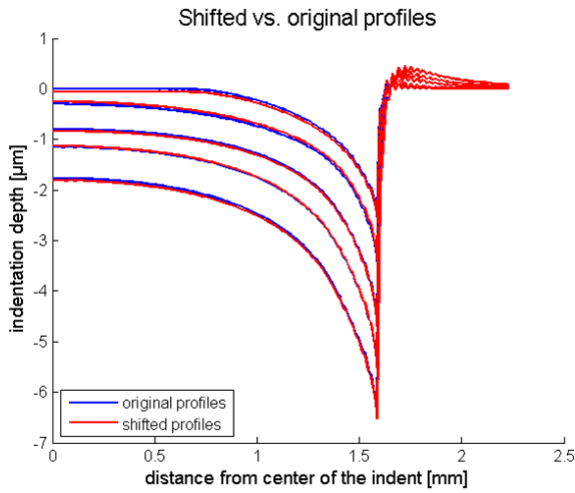


Figure 17: Shifted vs. original indentation profiles

		Relative error of identified parameters [%]				
Test		σ_{y0}	K	q_1	q_2	d
1.11	set 1	2.08	5.06	4.74	0.77	0.03
1.12	set 2	4.92	6.10	7.05	3.12	0.04
1.13	set 3	8.90	10.04	29.21	0.35	0.04
1.14	set 4	5.84	5.18	55.49	7.88	0.03
1.15	set 5	1.33	0.30	1.08	0.91	0.06

Table 7: Influence of variation in measurements on parameter identification

As a concluding remark of this present section we can say the following: The optimization by the Levenberg-Marquardt method works very well provided that the initial parameter set is sufficiently close to the solution. We ensure to provide an appropriate initial parameter set using a parametric approximation as explained in section 4 and 7. However, the identification of q_1 is not reliable as errors in the range of 20% can be observed. We propose to increase the number of indentation profiles used for inverse identification in order to increase the reliability of this parameter. In section 6.1 we could show that an erroneous estimation of the friction coefficient only has a limited effect on the inverse identification of all parameters. In section 6.2 we added white noise onto the

reference profiles in order to verify in how far the surface irregularities affect the inverse identification. We found that all parameters except for q_1 could be identified with sufficient accuracy. Similar results were found when studying the effect of a variation in measurements on the identification of parameters in section 6.3.

7. Results

The coatings' mechanical properties were determined from the parametric approximation and the Levenberg-Marquardt algorithm. For this purpose we selected 5 out of the 9 experimentally obtained indentation curves, namely those obtained at indentation loads of 10016N, 12024N, 14016N, 15017N and 16013N. As outlined in section 4 we first apply a parametric approximation in order to find a set of parameters $c^0 = (q_{1,0}, q_{2,0}, \sigma_{y0,0}, K_0, f_0)^T$ that is sufficiently close to the experimental profiles and which can serve as an initial guess for the Levenberg-Marquardt algorithm. We set $f_0 = 1.5\%$ and generate numerical indentation profiles for several parameter combinations that are in the following ranges: $200\text{MPa} < \sigma_{y0} < 1500\text{MPa}$, $5000 < K < 30000\text{MPa}$, $0.5 < q_1 < 3.0$, $0.5 < q_2 < 3.0$. For those combinations we found that $\sigma_{y0} = 1000\text{MPa}$, $K = 20000\text{MPa}$, $q_1 = 3.0$ and $q_2 = 3.0$ minimizes the error between numerical and experimental profiles. This set of parameters will hence serve as an initial guess for the Levenberg-Marquardt method. Furthermore, this set provides indentation profiles that are close to the experimental profiles (see figure 18) with $\Delta \approx 1\mu\text{m}$. In section 5 we have shown that the Levenberg-Marquardt algorithm even converges if the profiles' difference is $\Delta \approx 10\mu\text{m}$! For this reason we assume this initial parameter set to be sufficiently close to the solution as to guarantee convergence of the algorithm.

For the Levenberg-Marquardt algorithm applied to the experimental profiles we observed the following: Whilst for validation of the method by means of numerically generated profiles minimization of relative errors led to convergence towards the solution, this is not the case for the experimentally obtained indentation profiles. Here, convergence was only achieved when absolute

errors between the vertical displacements of iteratively generated and experimental curves were considered along the entire surface featuring 168 nodes. However, convergence towards a solution was achieved relatively quickly after as little as 3 iterations. This aspect is illustrated in figure 18 which depicts the indentation profiles for all iterations, the red line indicating the profile after the third iteration which comes sufficiently close to the experimental profile.

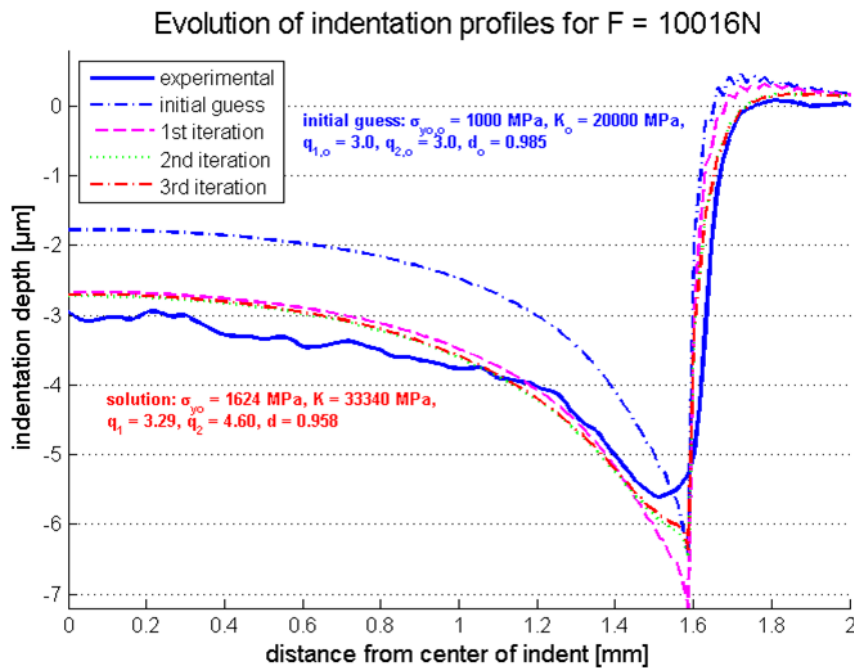


Figure 18 : convergence of indentation profiles for F = 16013N

The indentation profiles for all considered loads after the third iteration are depicted in figure 19. Most of the numerical indentation profiles correspond well with the experimental ones, with an exception of the profiles corresponding to an indentation load of 12024 N. The values for the parameters to be identified corresponding to the third iteration are as follows: $\sigma_{y0} = 1624$ MPa, $K = 33340$ MPa, $q_1 = 3.29$, $q_2 = 4.60$ and $f = 4.2\%$. As shown in section 4.3 of this work, nanoindentation tests provided an approximation to the yield strength at 0.2% plastic strain of about $\sigma_{y0} = 1930$ MPa when the top side of the sample was indented. The values for this parameter obtained by nanoindentation and the proposed method are hence relatively close to each other. However, the value for K obtained by nanoindentation only amounts to $K = 9300$ MPa whilst a value of $K = 33340$ MPa was obtained by the presented method. The void fraction obtained by this method

amounts to 4.2%. For comparison, the void fraction as measured by optical imagery amounts to 1.5% and that indicated on the technical data sheet ranges between 1-4%. It should be noted that the determination of volume fractions by means of optical imagery can be subject to significant errors that are mainly due to the quite subjective choice of the contrast threshold value that is taken as an indication for the presence of pores. In that sense the obtained value of 4.2% can still be considered to be a realistic value.

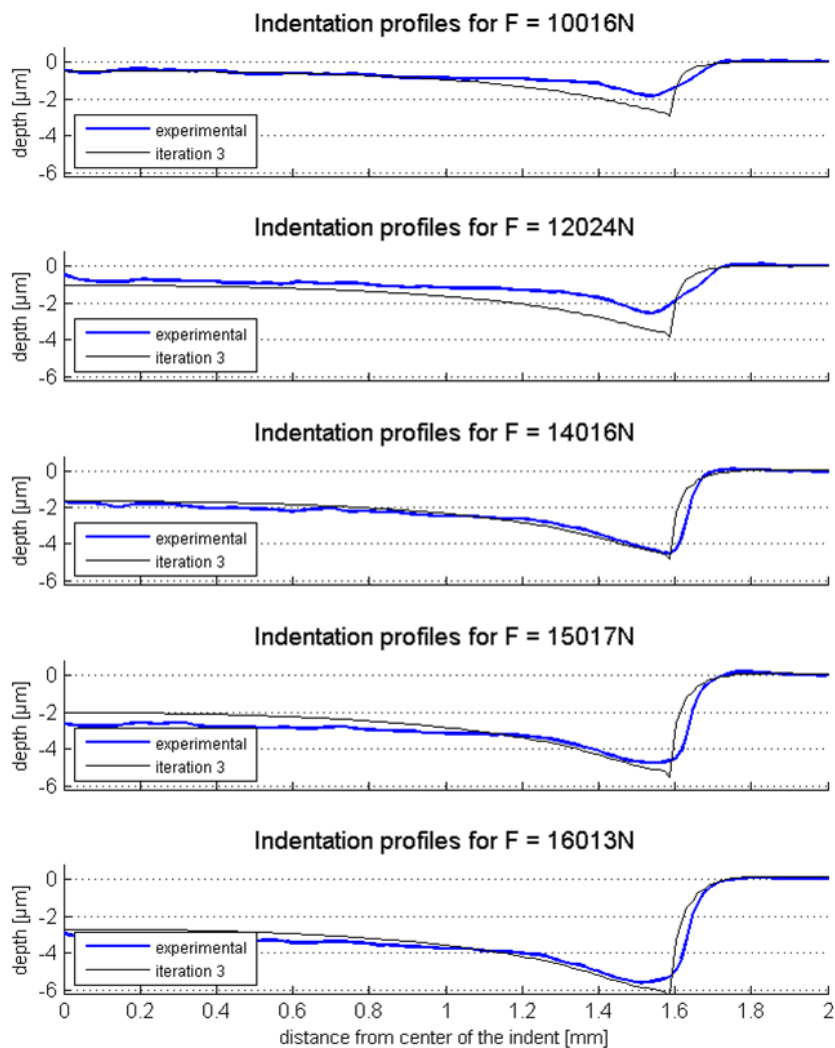


Figure 19 : iteratively generated indentation profiles after the third iteration vs. experimentally obtained profiles

8. Summary and conclusions

In this paper we proposed a novel inverse method for the identification of plastic properties of plasma-sprayed coatings by means of macro-indentation and the Levenberg-Marquardt algorithm. In contrast to conventional indentation techniques that require knowledge of the entire loading history the proposed method is based on the geometry of residual indents only which potentially makes it a powerful tool. The plastic properties of the coatings investigated in this study have been represented by the Gurson-Tvergaard plasticity criterion which is readily implemented in commercial finite element software such as Abaqus. The Levenberg-Marquardt algorithm created for the problem at hand aimed to fit numerically generated indentation profiles to the experimentally obtained ones. We could show that this method leads to a good fit between experimental and numerical results and that convergence towards a realistic solution is achieved after as little as three iterations.

Future work will be devoted to exploit the entire loading history in addition to the residual indents in order to retrieve elastic-plastic properties of plasma-sprayed coatings. Other indenter geometries will be considered in order to verify the proposed method. This method also allows the identification of material parameters at elevated temperatures since the influence of thermal expansion within the experimental setup is minimized. Future work will hence also include the identification of the coatings' properties at high temperature.

9. Acknowledgements

We would hereby wish to thank Airbus Operations S.A.S for funding this project.

References

- [1] Sevastianov, I and Kachanov, M. (2001); Plasma-sprayed ceramic coatings: anisotropic elastic and conductive properties in relation to the microstructure; cross-property correlations
- [2] Kroupa, F. and Plesek, J (2002); Nonlinear elastic behavior in compression of thermally sprayed materials
- [3] Sevastianov, I and Kachanov, M. (2004); Quantitative characterization of microstructures of plasma-sprayed coatings and their conductive and elastic properties
- [4] Kroupa, F. and Plesek, J (2002); Nonlinear elastic behavior in compression of thermally sprayed materials
- [5] Chicot, D. and Ageorges, H. (2014); Hardness of thermal sprayed coatings: relevance of the scale of measurement
- [6] Lourakis, M.I.A. (2005); A brief description of the Levenberg-Marquardt algorithm implemented by Ievmar
- [7] Gavin, H.P. (2013); The Levenberg-Marquardt method for nonlinear least squares curve-fitting problems
- [8] Springmann, M and Kuna, M. (2005); Identification of material parameters of the Gurson-Tvergaard-Needleman model by combined experimental and numerical techniques
- [9] Assire, A. (2013) Algorithmes de recalage
- [10] Taljat, B. and Pharr, G. (2004); Development of pile-up during spherical indentation of elastic-plastic solids
- [11] Habbab, H., Mellor, B. and Syngellakis, S.; Post-yield characterisation of metals with significant pile-up through spherical indentations
- [12] Clement, P., Meille, S., Chevalier, J; Mechanical characterization of highly porous inorganic solid materials by instrumented micro-indentation
- [13] Gu, Y., Nakamura, T. and Prehlik, L.; Micro-indentation and inverse analysis to characterize elastic-plastic graded materials
- [14] Chen, X.; Novel technique for measuring the mechanical properties of porous materials by nanoindentation
- [15] Karthik, V., Visweswaran P, Bhushan A.; Finite element analysis of spherical indentation to study pile-up/sink-in phenomena in steels and experimental validation
- [16] Tanstrum, M., Machta, B. and Sethna, J.; The geometry of nonlinear least squares, with applications to sloppy models and optimization
- [17] Oliver, W., Pharr, G. (2011); Measurement of hardness and elastic modulus by instrumented indentation: Advances in understanding and refinements to methodology

[18] Oliver, W., Pharr, G. (1992); An improved technique for determining hardness and elastic modulus using load and displacement sensing indentation experiments

[19] Zhang, C., Leng, Y. (2000); Elastic and plastic behavior of plasma-sprayed hydroxyapatite coatings on a Ti-6Al-4V substrate

[20] Prchlik, L., Pisacka, J. (2003); Deformation and strain distribution in plasma-sprayed nickel-aluminium coating loaded by a spherical indenter

[21] Tabor, D. (1951); Hardness of metals